Applied Catalysis A, General 566 (2018) 190–199

Contents lists available at ScienceDirect

Applied Catalysis A, General

journal homepage: www.elsevier.com/locate/apcata

A facile route for spraying preparation of Pt/TiO_2 monolithic catalysts toward VOCs combustion

Xiao Chen[a], Zhenglong Zhao[b], Ying Zhou[b], Qiulian Zhu[b], Zhiyan Pan[a,*], Hanfeng Lu[b,*]

[a] Institute of Environmental Chemicals and Resources, College of Environment, Zhejiang University of Technology, Hangzhou 310014, China
[b] Innovation Team of Air Pollution Control, Institute of Catalytic Reaction Engineering, College of Chemical Engineering, Zhejiang University of Technology, Hangzhou 310014, China

ARTICLE INFO

Keywords:
nano-Pt/TiO_2dispersion liquid
Monolithic catalysts
Dispersion-liquid-spraying method
Catalytic combustion

ABSTRACT

This study presents an efficient, economic, and simple preparation strategy for Pt/TiO_2 monolith catalysts. Nano-Pt/TiO_2 dispersion liquid with good activity and stability was synthesized by hydrolysis and chemical reduction method. Various Pt/TiO_2 monolithic catalysts were prepared by spraying the dispersion liquid on different substrates. Results of transmission electron microscopy, scanning electron microscopy, N_2 adsorption-desorption, H_2 temperature-programmed and CO oxidation showed that the Pt/TiO_2 nanoparticles with good mesoporous structure and redox properties were highly dispersed on the substrate. The as-prepared 0.5 Pt/TiO_2 cordierite monolithic catalyst with 0.1 wt‰ Pt content exhibited excellent catalytic combustion activity (T_{90} of toluene combustion was 212 °C), stability (no deactivation was observed during a 120 h test) and firmness (mass loss was 0.11% after 1 h ultrasonic vibration) under experimental conditions. Compared with state-of-the-art methods, this method is more suitable for large-scale production of waste-gas-treated monolith catalysts. And this method meets the concept of energy saving and emission reduction because of its simplicity, high efficiency, environmental friendliness, and high utilization of active components.

1. Introduction

The rapid development of industries led to a significant increase in volatile organic compounds (VOCs) emissions [1,2]. In addition to their toxicity, VOCs exposed to ultraviolet light in the atmosphere can cause ozone pollution and even photochemical smog pollution, which seriously harm the environment and human health [3–7]. The control of VOCs aroused tremendous attention. An increasing number of researchers are committed to eliminating VOCs.

Among the relevant techniques [8–12], such as adsorption, thermal incineration, photocatalytic degradation, plasma-catalytic oxidation, and catalytic combustion, catalytic combustion is a widely used technology for removing VOCs due to its advantages of less energy consumption, high treatment efficiency, absence of secondary pollution, and good environmental and economic benefits [13–18]. The most commonly used combustion catalysts are noble metal catalysts and complex metal oxides catalysts. Noble metal catalysts, which have superior catalytic activity, selectivity and universality, are the main catalysts in practical application. Pt-based materials are considered the most ideal catalyst for catalytic combustion [19–23]. He et al. prepared Pt/TiO_2 catalyst through impregnation method using anatase TiO_2 as support; they found that formaldehyde could be completely oxidized over the catalyst at room temperature [24]. Peng et al. synthesized Pt/HPMOR through impregnation method, wherein the T_{90} of toluene combustion was 190°C [25]. Santos et al. reported noble metal catalysts supported on TiO_2 by liquid-phase reduction deposition were active for the total oxidation of CO and VOCs [26].

However, the catalysts most widely used to treat industrial waste gases are monolithic ones because they offer great advantages over grained catalysts, such as improved mechanical properties and mass/heat transfer [27]. The preparation of monolithic catalysts presently involves the following steps. The washcoat is coated on the surface of the structured monolithic substrate followed by loading of active species through impregnation. Alternatively, the slurry prepared from powder catalyst is directly coated on the surface of the structured monolithic substrate, and the monolithic catalyst is obtained through activation treatment. The preparation process is cumbersome and the active components are easily lost, thereby leading to poor utilization ratio and increased preparation cost. Moreover, the active component in the prepared monolithic catalyst shows poor dispersion and adhesive strength, which seriously affect the activity and stability of the monolith catalyst [28]. Therefore, existing studies focus on reducing cost and

* Corresponding authors.
E-mail addresses: panzhiyan@zjut.edu.cn (Z. Pan), luhf@zjut.edu.cn (H. Lu).

https://doi.org/10.1016/j.apcata.2018.08.025
Received 14 June 2018; Received in revised form 10 August 2018; Accepted 27 August 2018
Available online 29 August 2018
0926-860X/

energy consumption and improving the efficiency of the monolithic catalysts in practical applications. A simple and efficient preparation strategy for monolithic catalysts must be adopted [29].

We reported a facile strategy for preparing monolithic catalysts through spraying method [30,31]. The present strategy focuses on the following points: preparing the nanoparticle (NP) dispersion liquid with catalytic activity for combustion through solvothermal method and spraying the dispersion liquid on the different substrates to obtain monolith catalysts. This strategy simplifies the preparation process of monolithic catalysts and improves the utilization of active components. Moreover, this strategy can reactivate catalysts when deactivated through respraying without replacing the monolithic catalysts. This process greatly minimizes hazardous waste generation and the costs of preparation and operation. In this study, active nano-Pt/TiO_2 dispersion liquid was synthesized through hydrolysis and chemical reduction method which is simpler and greener. The physical and chemical properties of Pt/TiO_2 NPs were characterized. And various Pt/TiO_2 monolithic catalysts were successfully prepared via simply spraying the dispersion liquid.

2. Experimental

2.1. Chemical agents

Tetrabutyl titanate ($C_{16}H_{36}O_4Ti$;TBT, CP) and acetic acid (CH_3COOH, AR) were purchased from Shanghai Lingfeng Chemical Reagent Co., Ltd. Chloroplatinic acid hexahydrate ($H_2PtCl_6{\cdot}6H_2O$, AR) was purchased from Aladdin. Ethyl alcohol absolute (CH_3CH_2OH, AR) was purchased from Anhui Ante Food Co., Ltd. Hydrazine hydrate ($N_2H_4{\cdot}H_2O$ 85%, AR) was purchased from Sinopharm Chemical Reagent Co., Ltd. P25 was purchased from Degussa AG. Polyethylene glycol (HO$(CH_2CH_2O)_nH$; PEG8000, AR) was purchased from Shanghai Macklin Biochemical Co., Ltd. Toluene (C_7H_8, AR) was purchased from Quzhou Juhua Reagent Co., Ltd.

2.2. Catalyst preparation

The nano-Pt/TiO_2 dispersion liquid and monolithic catalysts were prepared as follows (Fig. S1). The nano-Pt/TiO_2 dispersion liquid was synthesized via hydrolysis and chemical reduction. TBT (3.5 mL) was added to the mixed solution (30 mL of ethanol, 10 mL of acetic acid and 10 mL of deionized water) under stirring. The solution reacted by stirring at 40 °C for 5 h. The H_2PtCl_6 solution (2 mmol·L^{-1}; 0 mL, 2 mL, 10 mL) was added to the cooled homogeneous clear solution. The hydrazine hydrate solution (compound at once when using, 24 mmol·L^{-1}; 0 mL, 0.5 mL, 2.5 mL) was added by dropping during stirring. The resulting solution was diluted to 40 mL to obtain nano-Pt/TiO_2 dispersion liquid (20 mg mL^{-1}) after reacting at room temperature for 12 h. According to the mass ratio (0 wt%, 0.1 wt%, 0.5 wt%) of Pt to TiO_2, the Pt/TiO_2 dispersion liquids were denoted by TiO_2, 0.1 Pt/TiO_2, and 0.5 Pt/TiO_2.

Pt/TiO_2 powder catalysts were obtained via drying or calcination. The Pt/TiO_2 dispersion liquids dried at 110 °C were denoted by TiO_2-d, 0.1 Pt/TiO_2-d, and 0.5 Pt/TiO_2-d. These catalysts calcined at 400 °C for 3 h under air were denoted by TiO_2-c, 0.1 Pt/TiO_2-c, and 0.5 Pt/TiO_2-c.

Pt/TiO_2 monolithic catalysts were obtained through dispersion-liquid-spraying method. The 0.5 Pt/TiO_2 dispersion liquids (8 mL) were sprayed onto cordierite honeycomb (Φ 1.5 cm, h 5 cm, ~8 g). The resulting cordierite honeycomb (the mass ratio of Pt/TiO_2 to cordierite honeycomb: 2 wt%) dried at 110 °C was denoted by 0.5 Pt/TiO_2/CH (the mass ratio of Pt to cordierite honeycomb: 0.1 wt‰). This catalyst was calcined at 400 °C for 3 h under air and was denoted by 0.5 Pt/TiO_2/CH-c. The other Pt/TiO_2 monolithic catalysts (the mass ratio of Pt/TiO_2 to support: 2 wt%) were prepared by spraying a certain amount of 0.5 Pt/TiO_2 on reticulated SiC, foamed alumina, and brick. They were denoted as 0.5 Pt/TiO_2/SiC, 0.5 Pt/TiO_2/Al_2O_3, and 0.5 Pt/TiO_2/Brick. The catalysts calcined at 400 °C for 3 h under air were denoted by 0.5 Pt/TiO_2/SiC-c, 0.5 Pt/TiO_2/Al_2O_3-c, and 0.5 Pt/TiO_2/Brick-c.

R-Pt/TiO_2 monolithic catalysts were prepared through slurry-coating method. Certain amounts of P25 and polyethylene glycol (the mass ratio of PEG to P25: 1 wt%) were added to deionized water through stirring. The mixture was stirred at room temperature for 6 h to form TiO_2 slurry (0.02 g/mL). The cordierite honeycomb was impregnated with the slurry for 30 min and then dried at 110 °C for 5 h. This process was repeated three times. The TiO_2-coated cordierite honeycomb was calcined at 400 °C for 3 h under air. The content of TiO_2 on cordierite honeycomb was approximately 2 wt%. H_2PtCl_6 solution (3 mL, 2 mmol·L^{-1}) was diluted to 40 mL, and the TiO_2-coated cordierite honeycomb fully immersed into it for 24 h. The Pt/TiO_2-coated cordierite honeycomb dried at 110 °C was denoted by R-0.5 Pt/TiO_2/CH (the mass ratio of Pt/TiO_2 to support: 2 wt%). This catalyst was calcined at 400 °C for 3 h under air and was denoted by R-0.5 Pt/TiO_2/CH-c.

2.3. Catalyst characterization

A Tecnai F30 S-Twin transmission electron microscope operated at 300 kV was used for transmission electron microscopy (TEM). Samples for TEM investigation were prepared by dropping Pt/TiO_2 dispersion liquid onto a carbon-coated copper grid.

X-ray diffraction (XRD) patterns were recorded on a PANalytical X' Pert PRO diffractometer instrument operated at 40 kV and 30 mA, with Cu Kα-ray radiation (λ = 1.54178 Å). Scans were taken with a 2θ range from 10° to 80°.

Scanning electron microscopy (SEM) images were obtained on a Hitachi S-4700(II) microscope operated at 15.0 kV.

N_2 adsorption-desorption isotherms of the samples were carried out at 77 K on a Micromeritics ASAP2020 instrument. The specific surface areas and the mesopore sizes of the samples were calculated using the Brunauer-Emmett-Teller (BET) and Barrett-Joyner-Halenda (BJH) method, respectively. All samples were pre-treated in vacuum at 200 °C for 5 h before measurements.

H_2 temperature-programmed reduction (H_2-TPR) was measured on a FINE SORB-3010 E instrument equipped with a thermal conductivity detector (TCD). The sample was placed in a quartz reactor, pre-treated in Ar flow at 200 °C for 1 h and cooled down at 50 °C. The catalyst bed was performed by admitting a flow of 5 vol% H_2/Ar at 60 °C for 10 min, followed by heating at a constant rate (10 °C min^{-1}) up to 750 °C. Finally, the catalyst was cooled under the Ar flow. The flow rates in the experiment were 30 mL·min^{-1}. Hydrogen consumption was monitored using TCD operated at 60 °C and 60 mA.

Adhesion test was conducted by immersing the monolithic catalyst after calcination in deionized water inside a beaker and vibrating in an ultrasonic vibration instrument (40 kHz/100 w) for 10, 30, and 60 min. The sample was then dried at 110 °C, and a catalytic performance test for toluene combustion was performed. Mass loss was calculated according to the following equation:

$$\text{Mass loss} = (M_0\text{-}M_1)/M_0 \times 100\%$$

where M_0 and M_1 are the masses of the sample before and after ultrasonic vibration [32].

CO oxidation reaction was conducted in a fixed-bed microreactor. The powder catalyst was placed in a quartz reactor. Feed gas was 1 vol % CO balanced with air, and the gas flow rate was 40 mL min^{-1}. The CO concentrations were detected by a gas chromatograph equipped with TCD. The conversion of CO was obtained on the basis of CO consumption and calculated by the inlet and outlet concentrations of CO. The turnover frequency (TOF) value of CO oxidation calculated on the basis of dispersion of Pt NPs on the catalyst surface and the conversion rate of CO as

$$\text{TOF} = X_{CO}{\cdot}F_{CO}{\cdot}M_{Pt}/(m_{cat}{\cdot}X_{Pt}{\cdot}D_{Pt})$$

where X_{CO} is the conversion rate of CO, F_{CO} is the flow rate of CO (mol h^{-1}), m_{cat} is the mass of catalyst, X_{Pt} is the Pt content of catalyst, D_{Pt} is the dispersion of Pt (Table S1), and M_{Pt} is the molar mass of Pt.

2.4. Catalytic activity test

The combustion of toluene activity over these catalysts was evaluated with a continuous flow-fixed bed reactor. The feed consists of 2000 ppm toluene was generated by bubbling standard air through a bottle that contained pure toluene placed in an ice-water mixture (0 °C). The gas hourly space velocity (GHSV) was 3000 h^{-1} for cordierite honeycomb monolithic catalyst. The weight hourly space velocity (WHSV) was 34,000 mL g^{-1} h^{-1} for powder catalyst. For other monolithic catalysts, WHSV was 370,000 mL g^{-1} h^{-1} (based on the Pt/TiO_2 of the load). The concentrations of the toluene were detected by a gas chromatograph equipped with FID. The conversion of toluene was obtained on the basis of the inlet and outlet concentrations of toluene. The TOF value of toluene combustion was calculated similar to that of CO oxidation.

3. Results and discussion

3.1. Characterization of Pt/TiO_2 dispersion liquid and NPs

3.1.1. Dispersion and phase analysis of Pt/TiO2 dispersion liquid

The dispersion and phase analysis of Pt/TiO_2 dispersion liquid are shown in Figs. 1 and 2. Fig. 1a-1, b-1 and c-1 show the photos of all Pt/TiO_2 dispersion liquid. Obviously, all samples were uniformly transparent, which indicated that the NPs were highly dispersed in liquid. The color of dispersion liquid deepened with the increase in Pt addition, which implied that Pt was successfully reduced and highly dispersed in the system. The crystal structure of the particles in the liquid was verified by X-ray diffractometer. The results are shown in Fig. 2. The anatase TiO_2 with good crystallinity could be obtained by hydrolization of TBT. No characteristic peaks of Pt were observed in 0.1 Pt/TiO_2-d and 0.5 Pt/TiO_2-d (Fig. 2a). The samples after calcination also just exhibited diffraction peaks of anatase TiO_2 (Fig. 2b). The relatively small amount of the Pt in a highly dispersed form on the TiO_2 surface caused difficulty in XRD detection [33,34].

TEM was used to evaluate the dispersion state and the bonding form of the Pt/TiO_2 in the liquid. The TEM images (Figs. 1a-2–4, b-2–4 and c-2–4) show that the dispersion liquid would form a film on the surface of the substrate after drying. This formation is due to the fact that organics, such as acetic acid, are present in the dispersion liquid, and the TiO_2 NPs are connected to one another by the chelation of acetate when the concentration is high. TiO_2 NPs could be easily dispersed by dilution (Figs. S8a-1–3, b-1–3 and c-1–3), which indicated that the TiO_2 NPs prepared by this scheme were dispersed in the solution without reunion. Pt was introduced into the TiO_2 dispersion liquid by reduction of chloroplatinic acid using hydrazine hydrate as reducing agent. It could be observed that Pt NPs were dispersed on the surface of the TiO_2 film from TEM images of 0.5 Pt/TiO_2 (Figs. 1c-2–4 and S8c-1–3), but the presence of Pt was difficult to observe from TEM images of 0.1 Pt/TiO_2 (Figs. 1b-2–4 and S8b-1–4). However, the high-angle annular dark-field (HAADF)-TEM images (Fig. S9) illustrate that the smaller Pt NPs homodispersed on the surface of the TiO_2 film in 0.1 Pt/TiO_2. Table 1 lists the size and dispersion of Pt in 0.1 Pt/TiO_2 (2.5 nm, 45.2%) and 0.5 Pt/TiO_2 (27.6 nm, 4.1%) calculated from HAADF-TEM images. This phenomenon was due to Pt NPs aggregation growth as the amounts of chloroplatinic acid and hydrazine hydrate increased. In addition, observing the TEM and HAADF-TEM images of Pt-containing samples (Figs. 1b-2–4, c-2–4 and S8b-1–3, c-1–3), all Pt NPs appeared on the surface of TiO_2, which indicated that Pt was already combined with TiO_2 in the dispersion liquid. Fig. 1c-4 depicts that Pt NPs were

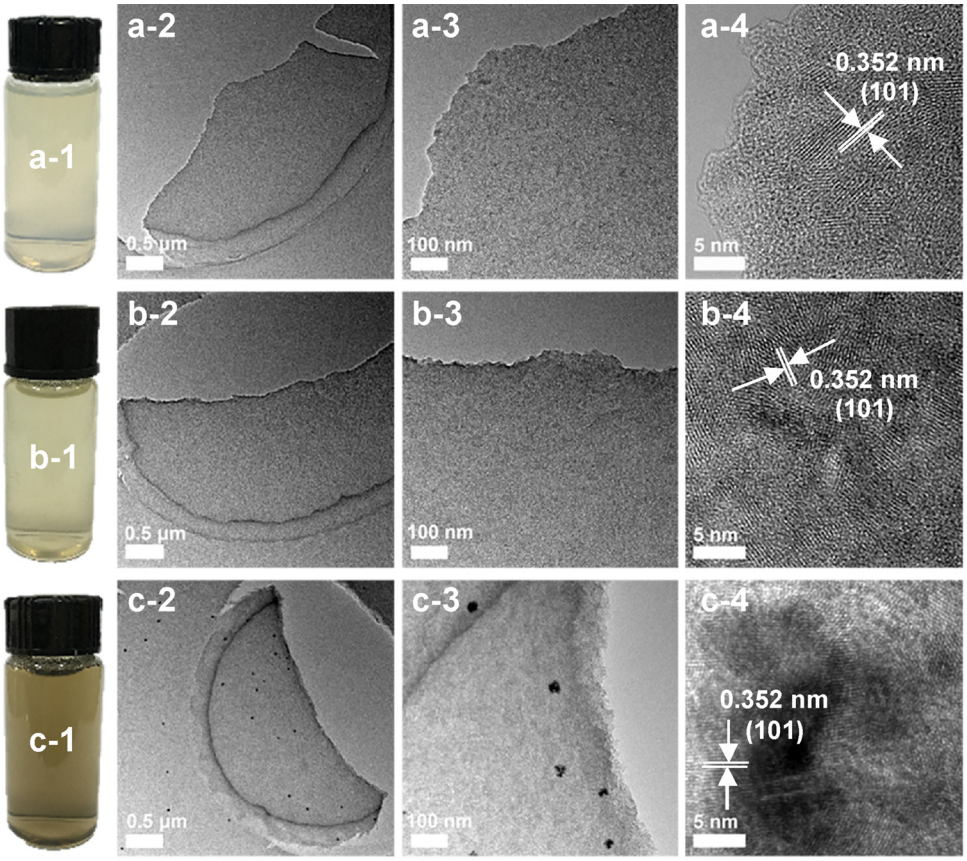

Fig. 1. The photos of TiO_2 (a-1), 0.1 Pt/TiO_2 (b-1) and 0.5 Pt/TiO_2 (c-1); TEM images of TiO_2 (a-2 ~ 4), 0.1 Pt/TiO_2 (b-2 ~ 4) and 0.5 Pt/TiO_2 (c-2 ~ 4).

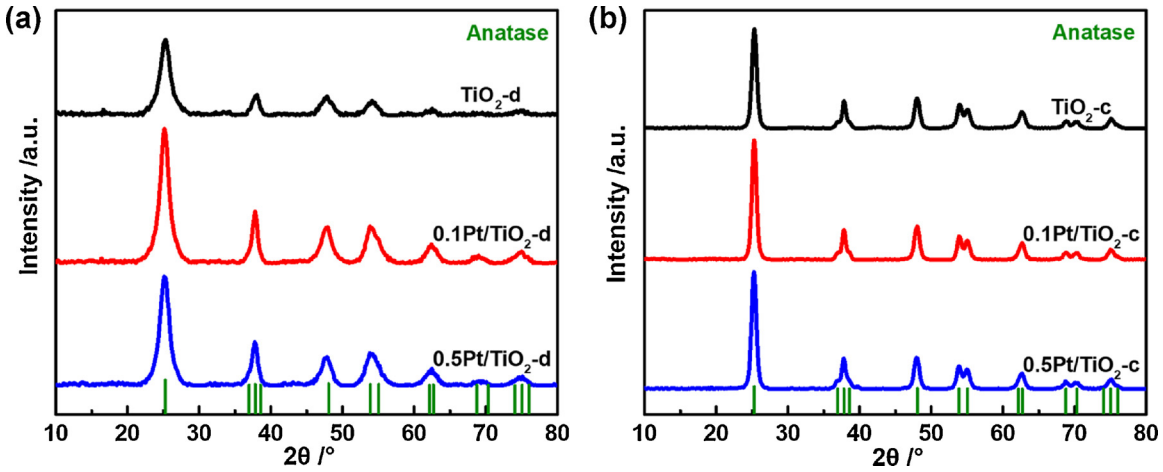

Fig. 2. XRD patterns of Pt/TiO_2 nanoparticles (a. uncalcined, b. calcined).

Table 1
The dispersion of Pt.

Sample	d(nm)	D(%)
0.1 Pt/TiO_2	2.5	45.2
0.5 Pt/TiO_2	27.6	4.1

supported on (101) plane of TiO_2. Hence, the NPs in the dispersion were in the form of Pt on the surface of TiO_2. The above characterization showed that the Pt/TiO_2 NP dispersion liquid can be easily obtained by the preparation strategy shown in Fig. S1a. An active film with active components uniformly dispersed on the substrate can be formed after spraying.

3.1.2. Textural properties of Pt/TiO2 NPs

The N_2 adsorption-desorption technique was adopted to evaluate the texture structure of Pt/TiO_2 NPs. Table 2 lists some information about textural parameters of the samples derived from N_2 adsorption-desorption. It could been found that the samples after calcination showed increased pore size and decreased pore volume and S_{BET}. This characterization was due to the pores with narrow necks and wide bodies (Fig. S10a), which originated from the aggregation of primary TiO_2 particles and the influence of organic matter, formed uniform and orderly cylindrical mesopores (Fig. S10c) when the organic matter was removed and the order degree increased with sample calcining. For calcined samples, the pore size, pore volume and S_{BET} decreased with the increase in Pt loading amount. This phenomenon can be elucidated as follows. First, the density of the samples increased with increasing Pt loading because of the higher density of Pt (21.45 $g{\cdot}cm^{-3}$) than that of TiO_2 (3.84 $g{\cdot}cm^{-3}$) given that the pore volume ($cm^3\,g^{-1}$) and S_{BET} ($cm^2\,g^{-1}$) expressed per gram of the sample. Second, Pt was perfectly dispersed on the surface of TiO_2 and partially blocked the mesopores, thereby resulting in decreased in pore size, pore volume and S_{BET} [35]. For uncalcined samples, the sequence of the pore size, pore volume, and S_{BET} is 0.1 Pt/TiO_2-d > 0.5 Pt/TiO_2-d > TiO_2-d. This phenomenon can be understood as follows. First, gas will be generated when hydrazine hydrate was added, which was obviously observed in preparation. Thus, the pore size, pore volume, and S_{BET} increased due to pore-making ability of gas. Second, pore size, pore volume, and S_{BET} decreased with the increase in Pt loading. Thus, the pore size, pore volume, and S_{BET} of 0.5 Pt/TiO_2-d slightly reduced than that of 0.1 Pt/TiO_2-d.

Table 2
Texture structure of Pt/TiO_2 nanoparticles.

Sample	Pore size (nm)		Pore volume ($cm^3\,g^{-1}$)		S_{BET}($m^2\,g^{-1}$)	
	d	c	d	c	d	c
TiO_2	3.4	9.4	0.26	0.27	303	113
0.1 Pt/TiO_2	4.5	9.3	0.37	0.26	334	109
0.5 Pt/TiO_2	4.1	9.1	0.33	0.24	323	106

d: NPs obtained by drying; c: NPs obtained by calcination.

In summary, the as-prepared Pt/TiO_2 NPs have good mesoporous structure (Fig. S10) and Pt dispersion, which is beneficial for the diffusion of the reactants and products. The activity must be improved, particularly for the relatively large molecules, such as toluene [36].

3.1.3. Chemical properties of Pt/TiO2 NPs

H_2-TPR was employed to investigate the redox capability of Pt/TiO_2 NPs, which is an important factor that affects catalytic reaction. Fig. 3 shows the H_2-TPR profiles of all Pt/TiO_2 NPs. For the TiO_2-d (Fig. 3a), the negative H_2-consumption peaks at approximately 280 °C and 458 °C could be attributed to the influence of organic matter. The temperatures of these negative H_2-consumption peaks were relative to weight loss temperature of organic on the sample (Fig. S11a). The H_2-consumption peak at approximately 342 °C might be caused by the reaction of organics and hydrogen. For instance, the hydrogenation of acetate induced hydrogen consumption (Fig. S11b) [37]. However, the negative H_2-consumption peak disappeared, and the trend of hydrogen consumption appeared at approximately 280 °C of 0.1 Pt/TiO_2-d and 0.5 Pt/TiO_2-d (Fig. 3a). This result was attributed to hydrogen spillover because of Pt. Another negative H_2-consumption peak at approximately 426 °C of 0.1 Pt/TiO_2-d and 0.5 Pt/TiO_2-d was due to back spillover. The H_2-TPR curves of 0.1 Pt/TiO_2-d and 0.5 Pt/TiO_2-d were approximately the same. Thus, they exhibited the similar redox capability, which explained similar CO oxidation and toluene combustion activity over these two Pt/TiO_2 NPs (Figs. 4a and 5 a).

The H_2-TPR curves of Pt/TiO_2 NPs after calcination are shown in Fig. 3b. The intrinsic redox capability of Pt/TiO_2 NPs was given with the removal of organics. Reduction peak was not observed on the TiO_2-c before 500 °C. H_2 consumption peaks at $T > 500$ °C were attributed to the reduction of bulk oxygen of TiO_2 [24]. The 0.1 Pt/TiO_2-c sample showed three H_2-consumption peaks before 500 °C. The H_2-consumption peak at approximately 148 °C was associated to the reduction of PtO_x crystallites to metallic Pt. Peak at approximately 290 °C could be attributed to hydrogen spillover because of Pt. The peak at approximately 432 °C might be caused by the reduction of the surface capping oxygen of TiO_2 [38,39]. These three reduction peaks also increased with increasing of Pt. For example, the two H_2-consumption peaks of 0.5 Pt/TiO_2-c between 200 °C and 500 °C formed a maximum reduction peak, which greatly enhanced the reduction of oxygen species on TiO_2

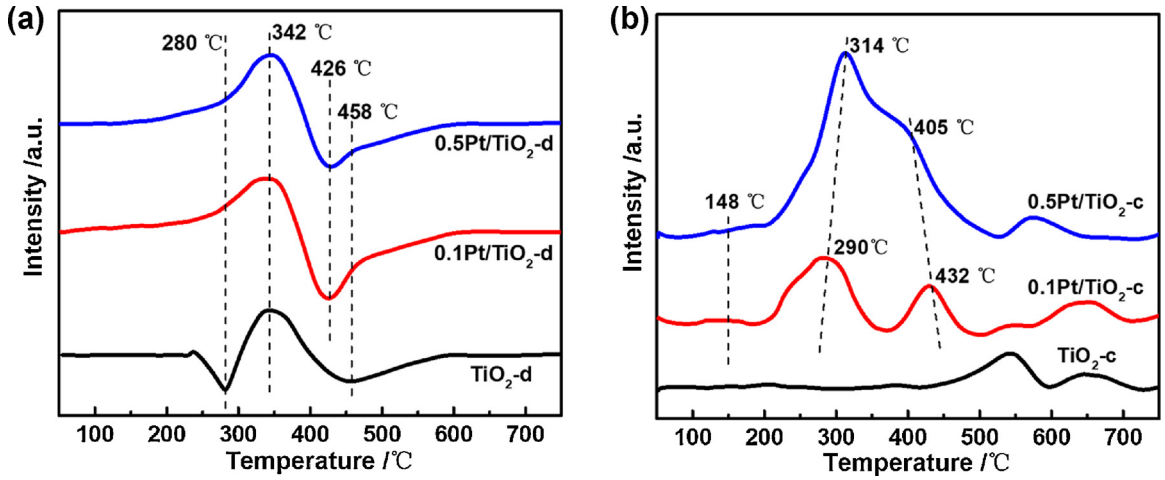

Fig. 3. H_2-TPR profiles of Pt/TiO_2 nanoparticles (a. uncalcined, b. calcined).

surface.

These results suggested that the as-prepared Pt/TiO_2 nanoparticles have good redox capability, which is beneficial for heterogeneous catalytic oxidation reactions [40].

CO oxidation is a structure-sensitive reaction and the reaction process is relatively simple. It is often used as the probe reaction to study the catalytic oxidation properties of catalysts in the scientific research field [41]. The light-off curves of CO oxidation are shown in Fig. 4a to understand the chemical properties of the as-prepared Pt/TiO_2 NPs. The CO oxidation activity over TiO_2-d was better than that of TiO_2-c. This result could be attributed to the agglomeration of TiO_2 NPs during calcination and indicated that the as-prepared NPs in dispersion liquid were highly dispersed and had certain catalytic activity. The CO oxidation results of Pt-containing samples also reflected the structure and physicochemical properties of Pt/TiO_2 NPs. The activity of 0.1 Pt/TiO_2-d was similar to that of 0.5 Pt/TiO_2-d because they had similar redox properties (Fig. 3a). The TOF values calculated on the basis of the exposed active sites of Pt NPs (Pt dispersion shown in Table 1), which implied that the TOF on 0.5 Pt/TiO_2-d was greater than on 0.1 Pt/TiO_2-d (Fig. 4b). Pt NPs were supported on the (101) plane of TiO_2 that exhibited strong interaction, which was beneficial for CO oxidation [42]. Although the increase in the amount of chloroplatinic acid and hydrazine hydrate caused aggregation growth and dispersion decreased of Pt NPs, it was important to enhance the interaction between Pt and TiO_2. This result could be identified by the H_2-TPR curves of Pt/TiO_2 nanoparticles after calcination (Fig. 3b). The enhancement of the interaction between Pt and TiO_2 as the Pt content further enhanced the CO oxidation activity and improved the catalytic capability of the single active site. Consequently, the 0.5 Pt/TiO_2-d sample exhibited a greater TOF value. The interaction between Pt and TiO_2 was further enhanced and the activity was increased with the removal of organics after calcination. Therefore, the 0.5 Pt/TiO_2-c sample exhibits the best CO oxidation performance. The mutual verification of the CO oxidation results and the above characterization data confirmed that Pt NPs have indeed bound to TiO_2 in the dispersion liquid. The strong interaction between Pt NPs and TiO_2 is beneficial for catalytic combustion.

3.2. Catalytic activity of Pt/TiO_2 NPs

Fig. 5a shows the catalytic activities of all powder samples for toluene combustion to evaluate the catalytic combustion properties of the fabricated Pt/TiO_2 NPs. The activity of Pt-containing samples was enhanced with the organics removed after calcination, which were consistent with CO oxidation. The 0.5 Pt/TiO_2-d sample exhibited larger TOF values than those of the 0.1 Pt/TiO_2-d sample (Fig. 5b). The catalytic combustion results showed that the nano-Pt/TiO_2 dispersion liquid with catalytic combustion activity could be successfully prepared by following the strategy in Fig. S1a, which ensured the follow-up preparation of catalytic combustion monolithic catalysts by simply spraying on different substrates.

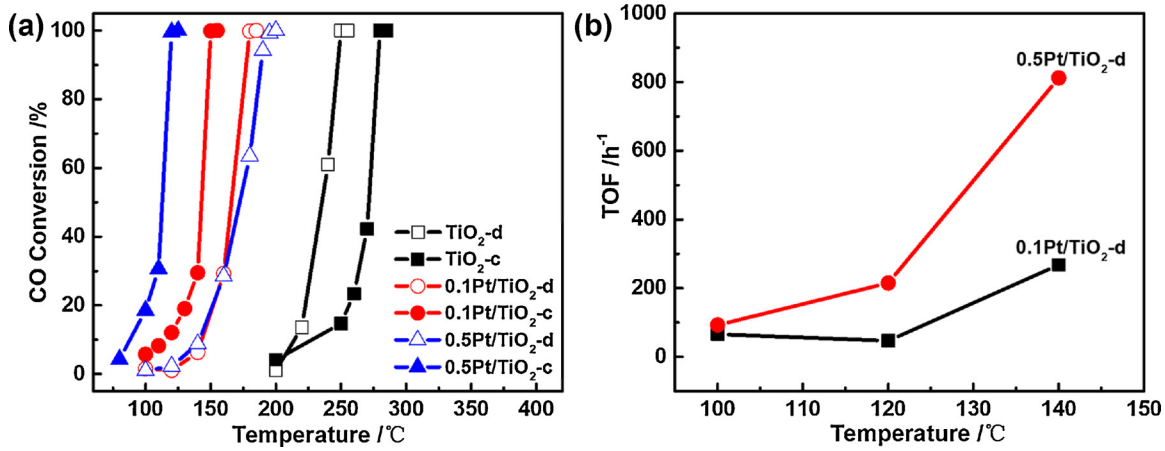

Fig. 4. (a) CO oxidation performance of Pt/TiO_2 nanoparticles. (b) TOF for CO oxidation on 0.1 Pt/TiO_2-d and 0.5 Pt/TiO_2-d. Reaction conditions: 1% CO, 21% O_2, balance N_2, WHSV = 24,000 mL g^{-1} h^{-1}.

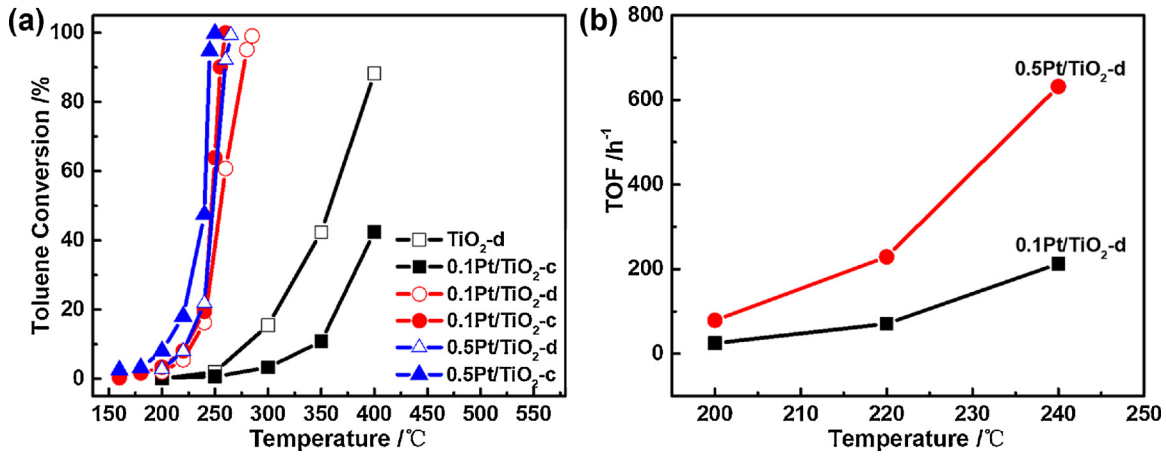

Fig. 5. (a) Toluene catalytic combustion performance of Pt/TiO_2 nanoparticles. (b) TOF for toluene combustion on 0.1 Pt/TiO_2-d and 0.5 Pt/TiO_2-d. Reaction conditions: 2000 ppm Toluene, 21% O_2, balance N_2, WHSV = 34,000 mL g^{-1} h^{-1}.

3.3. Properties of Pt/TiO_2 monolithic catalysts

3.3.1. Cordierite honeycomb substrate

The photos and SEM images of 0.5 Pt/TiO_2 cordierite monolithic catalysts are shown in Fig. 6. Unlike blank cordierite honeycomb, the cordierite surface was covered with a film after spraying the dispersion liquid. The highly dispersed active NPs could be clearly observed after removing organics by calcination, as shown in the SEM images. The same phenomenon was observed on the SEM images of the as-prepared monolithic catalysts based on reticulated sic, foamed alumina and brick (Fig. 10). The presence of organics in the dispersion liquid will lead to the formation of a Pt/TiO_2 active film after spraying on the substrate surface. The active NPs are dispersed in the film as in the dispersion liquid. The active NPs can be firmly dispersed on the surface when the organics are removed by calcination under the effect of the substrate. Therefore, the spraying of the active NP dispersion liquid, as shown in Fig. S1b, is an effective method for preparing a monolithic catalyst with excellent dispersibility of the active components. The dispersion of active components is an important factor that affects the catalyst performance [43–45]. Generally, the more dispersed the active components, the more active sites are exposed. Thus, the catalytic activity of the catalyst is improved. The monolith catalyst prepared only by simple spraying the active NP dispersion liquid on the substrate can obtain good catalytic performance.

Fig. 7a shows the toluene catalytic combustion activities of the monolithic catalysts prepared by different methods. Fig. 7b shows the temperatures that correspond to 10%, 50%, and 90% toluene conversion (T_{10}, T_{50}, and T_{90}, respectively). The catalytic activity of the Pt/TiO_2 cordierite monolithic catalysts prepared by our strategy was superior to the traditional slurry-coating method. In particular, the T_{10} of the monolithic catalyst prepared by our strategy was significantly lower than the slurry-coating method. For example, the T_{10} of 0.5 Pt/TiO_2/CH was 204 ℃, and R-0.5 Pt/TiO_2/CH reached 222 ℃. This phenomenon showed that the cordierite sprayed by the nano-Pt/TiO_2 dispersion liquid had considerable catalytic activity for toluene combustion without further calcination activation. Accordingly, the active NPs dispersion liquid spray method is a simpler and more effective energy-saving method for preparing monolith catalysts than the conventional method.

In addition to the catalytic performance of the monolith catalyst, the adherence of the active component on the substrate is also an important indicator for evaluating the catalyst. Adhesion test was conducted to study the firmness of the active components on the substrate (Fig. 8, Figs. S14 and S15). The loss curves of active components in Fig. 8a show that the curve of R-0.5 Pt/TiO_2/CH-c was steeper, which indicated the better firmness of active components on the substrate of the monolithic catalyst obtained by dispersion-liquid-spraying method. For example, after ultrasonic vibration for 60 min, the mass loss of 0.5 Pt/TiO_2/CH-c was only 0.11%, whereas that of R-0.5 Pt/TiO_2/CH-c was up to 0.64%. Furthermore, the catalysts after ultrasonic vibration were used for toluene catalytic combustion test (Fig. 8b). R-0.5 Pt/TiO_2/CH-c showed a significant decrease in activity after ultrasonic vibration, whereas 0.5 Pt/TiO_2/CH-c was able to maintain excellent activity. These results showed that although the monolithic catalyst prepared by dispersion liquid spraying is simple, the obtained monolithic catalyst shows improved firmness and activity, which is highly favorable for practical applications.

The stability of a catalyst is an important indicator for determining whether the catalyst can be used in practice. Cordierite monolithic catalysts were prepared with 0.5 Pt/TiO_2 dispersion liquid stored for 0, 10, 30, 60, and 100 days (Fig. S12a). The toluene catalytic combustion performances over these catalysts are shown in Figs. 9a and S16. T_{50} was constant similar to that in the NPs (Fig. S12b and S13). Therefore,

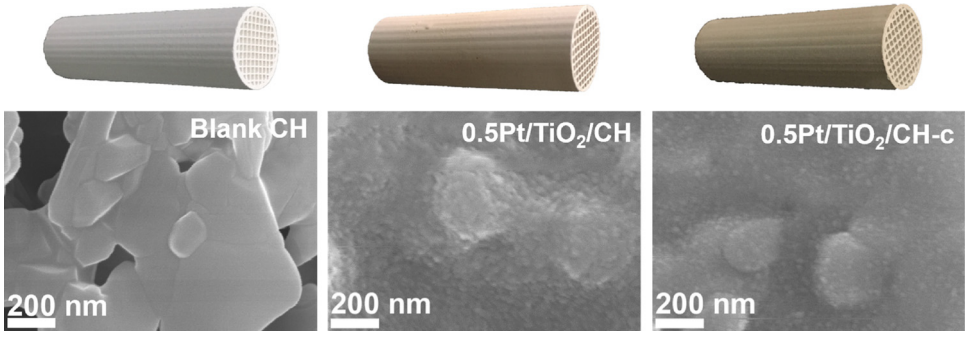

Fig. 6. The photos and SEM images of 0.5 Pt/TiO_2 cordierite monolithic catalysts.

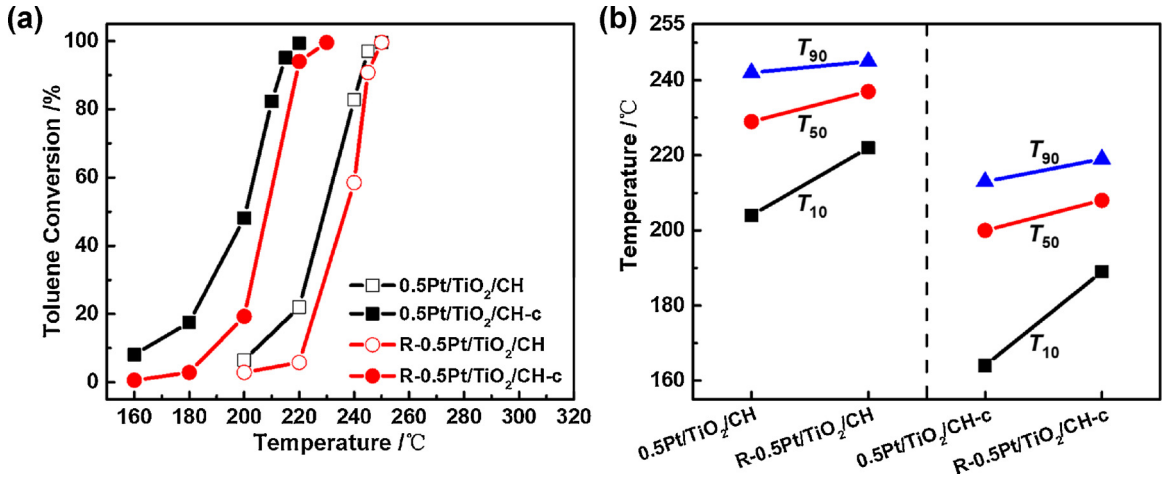

Fig. 7. (a) Toluene catalytic combustion performance of 0.5 Pt/TiO_2 cordierite monolithic catalysts prepared by different methods. (b) The T_{10}, T_{50} and T_{90} of toluene combustion over 0.5 Pt/TiO_2 cordierite monolithic catalysts prepared by different methods. Reaction conditions: 2000 ppm Toluene, 21% O_2, balance N_2, GHSV = 3000 h^{-1}.

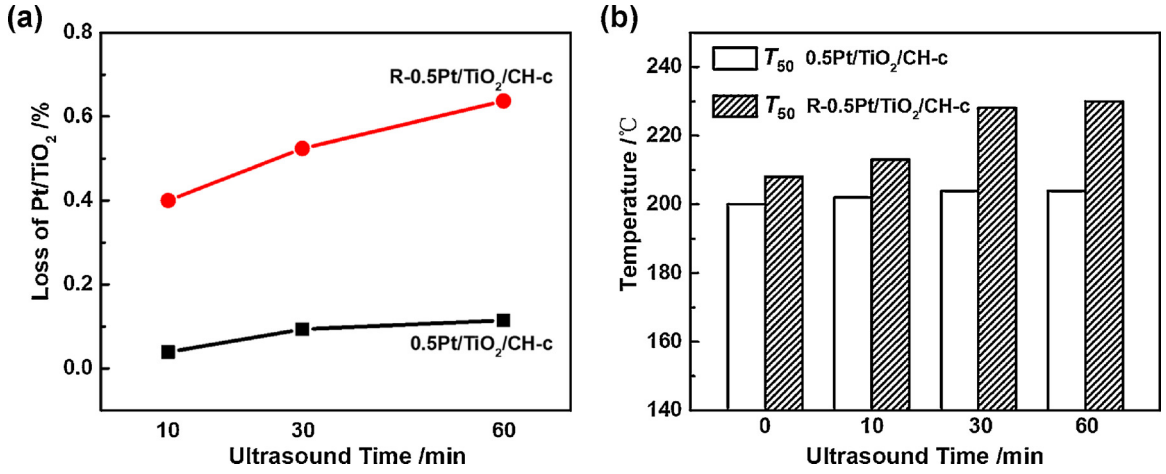

Fig. 8. The loss curves (a) and the toluene catalytic combustion T_{50} (b) of 0.5 Pt/TiO_2 cordierite monolithic catalysts prepared by different methods after ultrasonic vibration. Reaction conditions: 2000 ppm Toluene, 21% O_2, balance N_2, GHSV = 3000 h^{-1}.

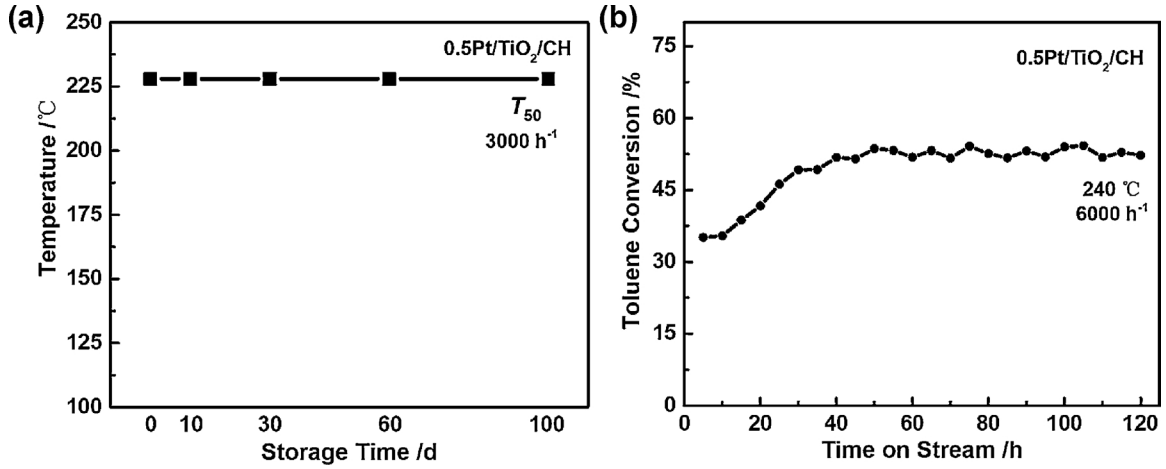

Fig. 9. T_{50} of 0.5 Pt/TiO_2/CH prepared with 0.5 Pt/TiO_2 stored for different time (a) and durability test of 0.5 Pt/TiO_2/CH (b) for toluene catalytic combustion; Reaction conditions: 2000 ppm Toluene, 21% O_2, balance N_2.

the long-time storage of the dispersion liquid did not affect subsequent spraying in preparing the monolithic catalyst. The long-time running stability test of 0.5 Pt/TiO_2/CH was evaluated at 240 °C and GHSV 6000 h^{-1}. The result shown in Fig. 9b. Toluene conversion increased with operation time in the early stage, because calcination could improve the catalytic activity as shown in Fig. 7. Then toluene conversion was maintained at about 50% during a nearly 80 h test. The as-prepared cordierite monolithic catalyst exhibits superior catalytic stability for

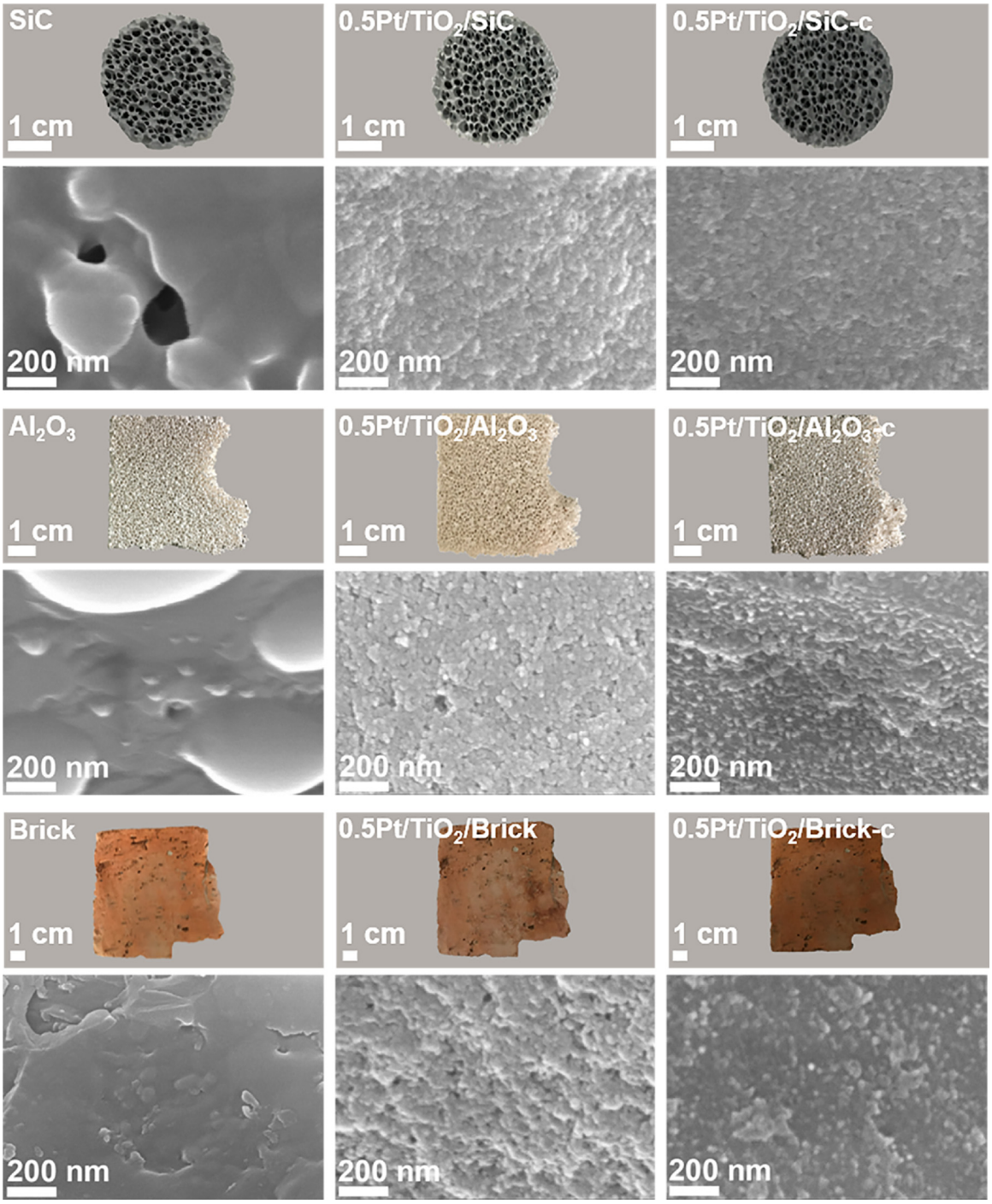

Fig. 10. The photos and SEM images of 0.5 Pt/TiO_2 monolithic catalysts with different substrates.

toluene combustion, which demonstrates the significant practical potential of our strategy.

3.3.2. Other substrates

Figs. 10 and 11 show the photos, SEM images, and toluene catalytic combustion performance of the monolithic catalysts with different substrates (reticulated SiC, foamed alumina, and brick) to illustrate that the preparation of Pt/TiO_2 monolithic catalysts using our strategy is facile and flexible. The catalytic combustion activities on these three monolithic catalysts were basically identical (Fig. 11). The complete combustion temperature of toluene over each uncalcined monolith catalyst was approximately 265 °C when WSHV was 370,000 mL $g^{-1}(Pt/TiO_2)\,h^{-1}$. The complete combustion temperature over these monolithic catalysts after calcination was approximately 240 °C. These phenomena strongly suggest that the active phases with relatively stable and good performance were formed in the as-prepared Pt/TiO_2 dispersion liquid and show that the substrate played a good role in supporting and dispersing the active components [46]. Fig. 10 shows that the active components were highly dispersed on the surface of every substrate. Hence, the active site could exhibit the same good catalytic activity on these three inactive substrates. The Pt/TiO_2 monolith catalysts with good catalytic combustion performance can be facile and flexibly prepared by spraying the dispersion liquid on various substrates. Therefore, this strategy is a universal and efficient method for preparing Pt/TiO_2 monolith catalysts.

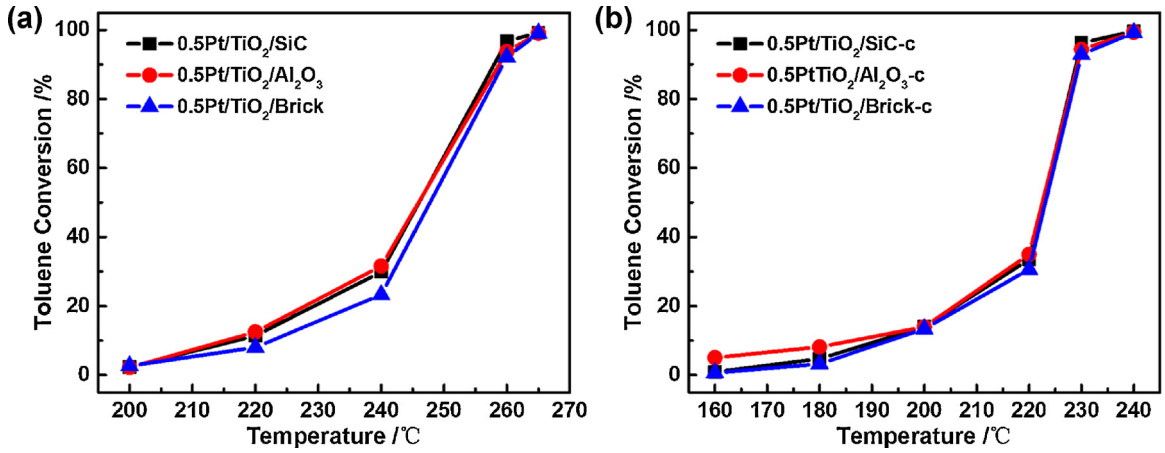

Fig. 11. The toluene catalytic combustion performance of 0.5 Pt/TiO_2 monolithic catalysts with different substrates (a: unroasted, b: calcined). Reaction conditions: 2000 ppm Toluene, 21% O_2, balance N_2, WHSV = 370,000 mL $g^{-1}(Pt/TiO_2)$ h^{-1}.

4. Conclusions

Nano-Pt/TiO_2 dispersion liquid with considerable activity was successfully fabricated by hydrolysis and chemical reduction method. TEM, N_2 adsorption-desorption, H_2-TPR and CO oxidation results show that the Pt/TiO_2 NPs in the dispersion liquid have good structure and redox properties. The TOF values and characterization results imply that the interaction between Pt and TiO_2 is an important factor that affects the catalytic capability of Pt/TiO_2. In the Pt/TiO_2 dispersion liquid, Pt NPs are supported on the (101) plane of TiO_2 that exhibits strong interaction. Therefore, the as-prepared Pt/TiO_2 dispersion liquid has good catalytic activity. Various Pt/TiO_2 monolithic catalysts are successfully prepared by simply spraying Pt/TiO_2 dispersion liquid on different substrates. SEM images show that the Pt/TiO_2 NPs are highly dispersed on the substrates. Compared with the Pt/TiO_2 monolithic catalysts prepared by slurry-coating method, those prepared by our strategy exhibit better firmness and toluene catalytic combustion performance. Moreover, the entire preparation process from dispersion liquid to the monolithic catalyst has no waste water discharge. Thus, our strategy does not cause loss of active components and significantly improves the economics of the precious metal catalyst. The preparation can be completed at a low temperature. This strategy meets the concept of energy conservation and emission reduction. Furthermore, the excellent stability of the Pt/TiO_2 dispersion liquid is suitable for long-time storage. The monolithic catalyst also shows superior long-term operating stability, which is favorable for practical application. The information acquired in this study may provide a new idea for the large-scale production of waste-gas-treated monolithic catalysts through a simple, friendly, efficient and economic strategy.

Acknowledgements

This work was supported by the Natural Science Foundation of China [NO. 21506194. 21676255]; the Natural Science Foundation of Zhejiang Province [NO. Y16B070011]; and the Commission of Science and Technology of Zhejiang province [NO.2017C03007, 2017C33106].

References

[1] X.T. Zeng, Y.F. Tong, L. Cui, X.M. Kong, Y.N. Sheng, L. Chen, Y.P. Li, J. Environ. Manage. 197 (2017) 507–521.
[2] B.A. Kathleen, R.T. Raymond, B.C. Alvin, B.C. Jose, J. Clean. Prod. 19 (2011) 187–196.
[3] J. Yoon, S.K. Chae, J.-M. Kim, J. Am. Chem. Soc. 129 (2007) 3038–3039.
[4] R.S. Peng, J.N. Pitts, Science 220 (2018) 462–470.
[5] T. Barakat, J.C. Rooke, E. Genty, R. Cousin, S. Siffert, B.-L. Su, Energy Environ. Sci. 6 (2013) 371–391.
[6] A.C. Lewis, N. Carslaw, P.J. Marriott, R.M. Kinghorn, P. Morrison, A.L. Lee, K.D. Bartle, M.J. Pilling, Nature 405 (2000) 778–781.
[7] A.L. Bolden, C.F. Kwiatkowski, T. Colborn, Environ. Sci. Technol. 49 (2015) 5261–5276.
[8] X.Y. Zhang, B. Gao, A.E. Creamer, C.C. Cao, Y.C. Li, J. Hazard. Mater. 338 (2017) 102–123.
[9] S. Salvador, J.M. Commandré, Y. Kara, Appl. Therm. Eng. 26 (2006) 2355–2366.
[10] X. Jia, X. Li, L. Xu, Y. Li, Q. Shi, T.T.L. Au-Yeung, C.W. Yip, X. Yao, A.S.C. Chan, Adv. Synth. Catal. 346 (2004) 723–726.
[11] M.B. Kizling, S.G. Järås, Appl. Catal. A Gen. 147 (1996) 1–21.
[12] M.S. Kamal, S.A. Razzak, M.M. Hossain, Atmos. Environ. 140 (2016) 117–134.
[13] C. Zhang, F. Liu, Y. Zhai, H. Ariga, N. Yi, Y. Liu, K. Asakura, M. Flytzani-Stephanopoulos, H. He, Angew. Chem. Int. Ed. 51 (2012) 9628–9632.
[14] H.F. Lu, X.X. Kong, H.F. Huang, Y. Zhou, Y.F. Chen, J. Environ. Sci. 32 (2015) 102–107.
[15] B. Bai, J. Li, ACS Catal. 4 (2014) 2753–2762.
[16] C.W. Ahn, Y.W. You, L. Heo, J.S. Hong, J.K.Jeon.Y.D. Ko, Y.H. Kim, H. Park, J.K. Suh, J. Ind. Eng. Chem. 47 (2017) 439–445.
[17] W. Tan, J. Deng, S. Xie, H. Yang, Y. Jiang, G. Guo, H. Dai, Nanoscale 7 (2015) 8510–8523.
[18] S. Cao, X.Q. Fei, Y.X. Wen, Z.X. Sun, H.Q. Wang, Z.B. Wu, Appl. Catal. A Gen. 550 (2018) 20–27.
[19] Y.F. Li, Y. Fan, J.M. Jian, L. Yu, G. Cheng, J.L. Zhou, M. Sun, Catal. Today 281 (2017) 542–548.
[20] B. Darif, S. Ojala, L. Pirault-Roy, M. Bensitel, R. Brahmi, R.L. Keiski, Appl. Catal. B-Environ. 181 (2016) 24–33.
[21] C. Chen, F. Chen, L. Zhang, S. Pan, C. Bian, X.M. Zheng, X.J. Meng, F.-S. Xiao, Chem. Commun. 51 (2015) 5936–5938.
[22] L. Gu, X. Chen, Y. Zhou, Q.L. Zhu, H.F. Huang, H.F. Lu, Chin. J. Catal. 38 (2017) 607–616.
[23] F. Diehl, J. Barbier, D. Duprez, I. Guibard, G. Mabilon, Appl. Catal. A Gen. 504 (2015) 37–43.
[24] C.B. Zhang, H. He, K. Tanaka, Appl. Catal. B: Environ. 65 (2006) 37–43.
[25] J.Y. Zhang, C. Rao, H.G. Peng, C. Peng, L. Zhang, X.L. Xu, W.M. Liu, Z. Wang, N. Zhang, X. Wang, Chem. Eng. J. 334 (2018) 10–18.
[26] V.P. Santos, S.A.C. Carabineiro, P.B. Tavares, M.F.R. Pereira, J.J.M. Órfão, J.L. Figueiredo, Appl. Catal. B: Environ. 99 (2010) 198–205.
[27] P. Avila, M. Montes, E.E. Miró, Chem. Eng. J. 109 (2005) 11–36.
[28] T. Vergunst, F. Kapteijn, J.A. Moulijn, Appl. Catal. A Gen. 213 (2001) 179–187.
[29] P. Avila, M. Montes, E.E. Miró, Chem. Eng. J. 109 (2005) 11–36.
[30] X. Chen, Q.Q. Xu, Y. Zhou, Q.L. Zhu, H.F. Huang, Z.Y. Pan, P.F. Zhang, S. Dai, H.F. Lu, ChemistrySelect 2 (2017) 9069–9073.
[31] H. Li, Y. Wang, X. Chen, S. Liu, Y. Zhou, Q.L. Zhu, Y.F. Chen, H.F. Lu, RSC Adv. 8 (2018) 14806–14811.
[32] H.F. Lu, Y. Zhou, H.F. Huang, B. Zhang, Y.F. Chen, J. Rare Earths 29 (2011) 855–860.
[33] X.D. Wu, L. Zhang, D. Wang, S. Liu, Z.C. Si, J. Fan, J. Hazard. Mater. 225-226 (2012) 146–154.
[34] D.Y. Yoon, E. Lim, Y.J. Kim, J.H. Kim, T. Ryu, S. Lee, B.K. Cho, I.S. Nam, J.W. Choung, S. Yoo, J. Catal. 319 (2014) 182–193.
[35] L.F. Qi, B. Cheng, J.G. Yu, W.K. Ho, J. Hazard. Mater. 301 (2016) 522–530.
[36] S. Li, A. Tuel, F. Meunier, M. Aouine, D. Farrusseng, J. Catal. 332 (2015) 25–30.
[37] M.C. Zhou, H.T. Zhang, H.F. Ma, W.Y. Ying, Fuel Process. Technol. 144 (2016) 115–123.
[38] N.S.D. Resende, J.G. Eon, M. Schmal, J. Catal. 183 (1999) 6–13.
[39] B. Ouyang, S.H. Xiong, Y.H. Zhang, B. Liu, J.L. Li, Appl. Catal. A Gen. 543 (2017) 189–195.
[40] H.F. Lu, P.F. Zhang, Z.A. Qiao, J.S. Zhang, H.Y. Zhu, J.H. Chen, Y.F. Chen, S. Dai, Chem. Commun. 51 (2015) 5910–5913.
[41] I. Kocemba, J. Rynkowski, J. Gurgul, R.P. Socha, K. Łątka, J.M. Krafft, S. Dzwigaj, Appl. Catal. A Gen. 519 (2016) 16–26.

[42] Y. Zhou, D.E. Doronkin, M.L. Chen, S.Q. Wei, J.D. Grunwaldt, ACS Catal. 6 (2016) 7799–7809.
[43] J. Ying, H. Peng, X. Xu, R. Wang, F. Yu, Q. Sun, W. Liu, Z. Gao, X. Wang, Catal. Sci. Technol. 6 (2016) 5405–5414.
[44] Z. Abdelouahab-Reddam, R.E. Mail, F. Coloma, A. Sepúlveda-Escribano, Appl. Catal. A Gen. 494 (2015) 87–94.
[45] X. You, X. Wang, Y. Ma, J. Liu, W. Liu, X. Xu, H. Peng, C. Li, W. Zhou, P. Yuan, X. Chen, ChemCatChem 6 (2014) 3377–3386.
[46] J.M. Gatica, J. Castiglioni, C.D.L. Santos, M.P. Yeste, G. Cifredo, M. Torres, H. Vidal, Catal. Today 296 (2017) 84–94.